ELSEVIER

Chemical Engineering Science 60 (2005) 2785–2794

Chemical Engineering Science

www.elsevier.com/locate/ces

Design of fluidized bed photoreactors: Optical properties of photocatalytic composites of titania CVD-coated onto quartz sand

Roberto L. Pozzo, Rodolfo J. Brandi, José L. Giombi, Miguel A. Baltanás*, Alberto E. Cassano

Instituto de Desarrollo Tecnológico para la Industria Química, Universidad Nacional and CONICET, Güemes 3450, S3000GLN Santa Fe, Argentina

Received 21 May 2004; received in revised form 6 December 2004; accepted 16 December 2004

Abstract

Volumetric optical properties (spectral absorption, scattering and extinction coefficients) of differently expanded narrow-path fluidized beds (FB) of a photocatalyst obtained by plasma-CVD deposition of titania onto quartz sand, relevant for photoreactor design purposes, are determined by using an unidirectional and unidimensional (1DD) model for the solution of the radiative transfer equation (RTE). Two simplified approaches are used: a Kubelka–Munk (KM) type of solution, by which the RTE is transformed into a pair of ordinary differential equations, and a discrete ordinate method (DOM) by which the complete RTE is transformed into an algebraic system that can be solved computationally. The second approach was validated by introducing the obtained optical parameters into a more elaborated bi-directional and two-dimensional (2DD) DOM model. Despite its simplicity, the KM method was able to yield fair order-of-magnitude estimates of the spectral optical properties of these FB.

Keywords: Fluidized beds; Optical parameters; Titania; Plasma-CVD coating

1. Introduction

A systematic research effort is being carried out by our group on the potentiality of fluidized beds (FB) of granular supports coated with titanium dioxide, as an alternative to titania slurry systems for UV photocatalytic oxidation of water pollutants, to minimize downstream separation costs. Our first approach (Pozzo et al., 1999, 2000) was an assessment of the relative performances of *the same* supported vs. slurried photocatalyst: A fluidized bed of a model material (Degussa P-25), immobilized onto quartz sand by dry/wet physical deposition, was studied in a fully illuminated photoreactor (FIP). The photoreactor was a multitube device, with three concentric annuli: The central annulus (7.5 mm of radial gap) was the reacting space; the outer one was an actinometric space, and the inner annulus was an IR filter. For the same catalyst loading inside the reacting space the slurry was about five times more active. The relatively poor photocatalytic performance and mechanical unstability of this titania–quartz composite (the TiO_2 peeled off after more than 12 h of reaction) lead us to plasma-CVD-coated glass beads as a novel alternative (Karches et al., 2002). More resistant, well adherent thin titania films could be obtained by this method, although their photocatalytic performance was similar or even lower than that of P25 immobilized on quartz sand. Apparently, Na migration from the glass beads, by thermally induced diffusion while calcining the amorphous plasma-generated TiO_2 (to induce crystallization), had a deleterious effect upon the catalytic properties of the composite.

Lately, by testing instead a plasma-CVD-coated quartz sand in the annular FIP reactor, a significant improvement in the photocatalytic performance was obtained. Furthermore, the new material showed a remarkable mechanical resistance

* Corresponding author. Tel.: +54 342 455 9175; fax: +54 342 455 0944.
E-mail addresses: tderliq@ceride.gov.ar, tderliq@arcride.edu.ar (M.A. Baltanás).

0009-2509/$ - see front matter © 2005 Elsevier Ltd. All rights reserved.
doi:10.1016/j.ces.2004.12.030

to abrasion. Yet, up to this point, our focus was primarily on the granular photocatalytic composites and their performance. Accordingly, relatively high concentrations of a well studied, model reactant (oxalic acid, 50 mM), to work under a pseudo-zero-order reaction regime, were used. After being confident with the good performance of the TiO_2–quartz composite, under FIP reactor conditions and pseudo-zero-order reaction regime, the next step was to remove those restrictions to rationalize (model) the system behavior. Two main goals were set:

- to be able to completely describe (evaluate) the radiation field inside the reactor, by determining the relevant optical parameters (scattering and absorption coefficients) of the two-phase system constituted by the narrow-channel fluidized bed of photocatalytic particles, and
- to extend the reaction kinetic studies for the model reactant in a wide range of concentrations, specially outside the pseudo-zero-order reaction limit.

Therewith, a research program was designed aiming to the combined modeling of the radiation field and the reaction kinetics in these narrow-channel FB systems. A double purpose, parallel planar reactor was built, so that it could be used either for the kinetic studies or as a part of an optical-spectrophotometrical assembly. To assess the scattering and absorption coefficients of the FB of the catalytic TiO_2–quartz composite, the optical assemblage included two integrating reflecting spheres, to measure the exiting radiation (forward and backward) from the FIP reactor. Experimental as well as methodological details for determining said optical parameters are discussed and evaluated in the present work. Kinetic modeling is the subject of another paper in progress.

In order to obtain relevant spectral (i.e., monochromatic) scattering and absorption coefficients from the spectrophotometrical measurements two approaches are compared: In the first approach, the radiative transfer equation (RTE), a mathematical expression of integro-differential nature, is transformed into a pair of ordinary differential equations that can have an analytical solution upon the introduction of simplifying assumptions with regards to the angular distribution of radiation intensity. In the second approach, the discrete ordinate method (DOM) is used to solve the complete RTE, by transforming the integro-differential equation into a complex algebraical system, which can be solved by computational calculations. In both approaches a model of plane-parallel layers perpendicular to a given axial direction was adopted for the radiation field, assuming that radiation properties are independent of the azimuthal angle ϕ and only a function the polar angle θ. The hereby-obtained optical parameters were then verified by introducing them into a more elaborated two-dimensional (2D) model for the reactor/optical cell.

2. Experimental work

2.1. Experimental set-up

A planar reactor, consisting basically of a hollow, rectangular frame of aluminum that left a 7.0 mm optical gap, and two optically clear 3.0 mm thick Tempax® borosilicate glass walls (36.0 cm height and 7.0 cm width) attached to it, was utilized as the cell for optical measurements (Fig. 1). The cell was vertically divided into two compartments by a grid of teflon: the upper one (21 cm high), where the FB of the TiO_2–quartz sand catalyst composite were developed, and the lower one filled with glass grains, for lessening jet formation in the bed zone immediately above the grid.

As indicated in the Introduction section, to assess the scattering and absorption coefficients of the catalytic composite in the FBs, the assemblage included two integrating reflecting spheres, one on each side of the cell, to collect the exiting backward (reflected) and forward (transmitted) radiation, from the illuminated reactor. A monochromatic, collimated light beam travels across the first sphere (R), irradiating a circular area of the front wall window of cell (beam diameter, $D_B = 8.8$ mm), right at the center of the FB. Said reflecting sphere (R) is able to collect the reflected radiation from the FB, while the second one (T), placed right after the second reactor wall, receives the radiation transmitted (extinguished) through the cell (Fig. 1).

Each sphere ($D_i = 12.0$ cm) was crafted by joining two hollow hemispheres machined from cubic pieces of aluminum. The interior of both spheres was coated with a water-based Munsell® (1.5 mm thick) reflecting paint. Sphere R was furnished with three radiation ports: port A directly faced the front reactor glass window, port B was located on the opposite side of the sphere, just at the exit the collimator, and port C at the top of the sphere, connecting to the photomultiplier detector of the spectrometer. Sphere T had also three ports, but only two were open under the measurement arrangement: port A' in line with port A of sphere R, facing the back reactor window, and port C' in a similar position as port C in sphere R, also linking to the spectrophotometer detector if needed. All ports were of 18 mm diameter. Both spheres were provided with a suppressor screen (S) to filter direct reflecting light on the detector. A pair of leveled, parallel steel rail tracks supported the spheres, allowing to change their relative distance at will, so that they could be placed either just in contact with the cell, in situation of measurement, or separate enough to allow the positioning of the cell.

A stable fluidized bed, at any given expansion, requires maintaining a steady flow. This condition was achieved by means of a constant hydrostatic pressure generation device consisting of two ‘open-atmosphere’ recirculating loops (Fig. 1): The main loop (I) included the cell reactor (1), an upper reservoir (2) supported by a jack mechanism for height control, to set a constant flow rate of the recirculating liquid (pure water), with a centered evacuating tube constantly

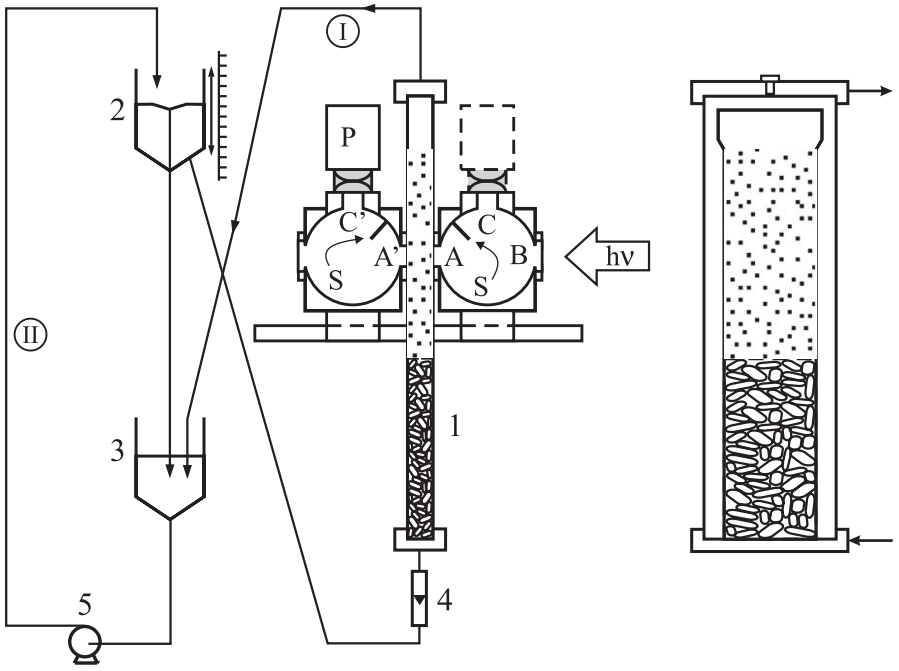

Fig. 1. Experimental set-up: (I) main water-recirculating circuit, (II) auxiliary circuit, (1) plane photoreactor/optical cell, (2) reservoir, (3) reservoir, (4) flow-meter, (5) peristaltic pump, (R) reflectance-collecting sphere, (T) transmittance-collecting sphere.

discharging on a second, lower reservoir (3) and a flow meter (4). The auxiliary loop (II), involved both reservoirs, and a peristaltic pump (5) to ensure a high recirculating flow of water.

The generation of the incident collimated light beam and the detection of forward and backward (sphere-integrated) outgoing UV radiation from the cell were carried out with an Optronic OL series 750 spectrophotometer, equipped with a double monochromator and interfaced with a data station. The radiation wavelength was varied in the 320–400 nm range. The lower wavelength limit is determined by the significant absorbance of Tempax® glass for $\lambda < 320$ nm.

2.2. Materials and methods

The catalyst composite was prepared by low-temperature CVD-plasma coating of Aldrich white quartz sand [Cat. no. 27,473-9; $\rho_s = 2.4\,\mathrm{g\,cm^{-3}}$; $D_p = 250\,\mu\mathrm{m}(+50-70\,\mathrm{mesh})$] with a thin, compact film of TiO_2 (by using Ti *t*-butoxide as precursor) in a vacuum-operated circulating fluidized bed reactor. More details about the preparation methods are given in Karches et al. (2002). The TiO_2 loading was determined by dissolving the films in a 10 wt% solution of $(NH_4)_2SO_4$ in concentrated H_2SO_4 and subsequent quantification by elementary analysis.

Three degrees of expansion of the FB, expanding always up to the same geometrical level in the cell (see Fig. 1), were employed: 7.0, 6.0 and 5.0 times the unexpanded bed volume (from now on these expansion degrees will be designated as: Ex 7, Ex 6 and Ex 5, respectively). Aliquots of 20.0, 23.0 and 28.0 g of the TiO_2–coated quartz sand were employed for each different expansion type, respectively. For comparison purposes, FB of the highly reflecting bare quartz sand with identical expansion degrees were also tested. All measurements were done by triplicate, averaged and normalized. The normalization was made against 100% reflectance values measured (at each wavelength) using sphere R, which were taken by placing a thick layer of powdered $BaSO_4$ behind a 3.0 mm piece of Tempax® glass against port A of the sphere. This 100% spectral reflectances (R_{100}) were considered as representative of the incident radiation flux for each wavelength of the defined range. The corresponding normalized spectral values for 100% transmittance (T_{100}), were defined as the fotomultiplier current measured from the port C' of sphere T when the cell was full of ultrapure water. Prior to the experimental measurements a calibration was made, for the complete wavelength span, by interchanging the spheres (i.e., placing sphere T at the exit of the colimator), to correct the T_{100} data for geometrical and reflectance differences between the spheres.

Two kind of measurements were made, in terms of detector currents: the monochromated radiation back-reflected from the fluidized bed into the cell, captured by the detector as diffuse reflectance from sphere R, and the light transmitted through the cell and collected by the detector, also as diffuse reflectance, from the top opening of sphere T. All the measurements were referred to R_{100}, by determining the percent reflectance and transmittance (henceforth R_λ% and T_λ%) as the per cent ratios between the photometric currents measured at each wavelength in spheres R and T, and the R_{100} current, respectively.

Due to the high sensitivity of the detector (dark current in the order of 10^{-10} Å) all measurements were carried out in 'darkroom conditions'. Notwithstanding, an additional correction was made, by subtracting to each measured current the "black currents" registered by the detector in sphere R when the cell was filled with pure water only, and sphere T was replaced by a black light trap (a black cone).

3. Modeling and data processing

A theoretical frame for the evaluation of the optical parameters of an irradiated nonemitting, participative medium is given by the general equation for radiation transfer (RTE) at steady state (Ozisik, 1973)

$$\frac{\mathrm{d}I_\lambda(s,\underline{\Omega})}{\mathrm{d}s}+[\kappa_\lambda(s)+\sigma_\lambda(s)]I_\lambda(s,\underline{\Omega}) = \frac{1}{4\pi}\sigma_\lambda(s)\int_{4\pi}p(\Omega'\to\Omega)I_\lambda(s,\underline{\Omega})\,\mathrm{d}\Omega, \quad (1)$$

where $I_\lambda(s,\Omega)$ is the spectral specific intensity of radiation having a wavelength λ (between λ and $\lambda+\mathrm{d}\lambda$) and a direction of propagation characterized by the unit vector $\underline{\Omega}$, at location s in space, κ_λ is the spectral volumetric absorption coefficient, σ_λ is the spectral volumetric scattering coefficient and p is the phase function (photon scattering distribution function), which describes the probability that a ray from any direction $\underline{\Omega'}$ will be scattered into the particular $\underline{\Omega}$ direction for which the RTE is written.

To find a solution to the integro-differential equation (1) is not, in general an easy task since it implies, at each spatial point, integrating over the solid angle Ω, for all possible directions coming from the entire spherical space. For polychromatic radiation, an integration over the wavelength range of interest must also be performed.

The problem can be simplified if the system allows to be modeled as plane-parallel layers perpendicular to a given axial direction, being the radiation properties only dependent on the polar angle θ, but not on the azimuthal angle ϕ. Thus, the FB can be modeled as a rectangular space confined between the two parallel transparent optical windows if the incident radiation arrives perpendicularly from the collimated beam, upon the front plane of the cell. Therewith, a rectangular geometry can be assumed and a simplified model can be utilized, with a single directional variable (the polar angle θ or, instead, $\mu=\cos\theta$), because of the beam characteristics compatible with an azimuthal simmetry. Accordingly, the RTE can be reformulated as in Eq. (2) with boundary conditions given by Eqs. (3) and (4):

$$\mu\frac{\partial I_\lambda(x,\mu)}{\partial x}+\beta_\lambda I_\lambda(x,\mu)=\frac{\sigma_\lambda}{2}\int_0^1 p(\mu_0)I_\lambda(x,\mu')\,\mathrm{d}\mu', \quad (2)$$

$$I_\lambda(x=0,\mu)=I_\lambda^0, \quad \mu>0, \quad (3)$$

$$I_\lambda(x=d,\mu)=0, \quad \mu>0, \quad (4)$$

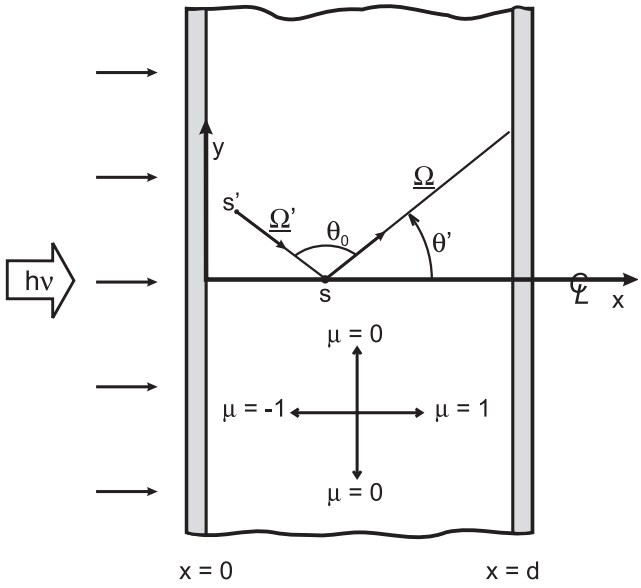

Fig. 2. Schematic diagram of the angular relationships among incident and scattered beams and the propagation direction of radiation, at any point in the fluidized bed.

where $\mu'=\cos\theta'$(θ' is the angle between any dispersed beam and the penetration direction x), $\mu_0=\cos\theta_0$ (θ_0 is the angle between an incident beam and any other dispersed beam), d is the total thickness of the medium (viz., the fluidized bed) and $\beta_\lambda=\kappa_\lambda+\sigma_\lambda$ is the volumetric spectral extinction coefficient (see Fig. 2).

As it is well known, geometrical optics can be used for the modeling of light scattering in a system of dispersed particles in a fluid medium whenever the so-called size parameter $x_{\mathrm{dc}}=\pi n_\lambda D_p/\lambda$ is greater than 5 (Ozisik, 1973). Since in our case the average particle diameter of the quartz sand ($D_p=250\,\mu\mathrm{m}$) is about three order of magnitude larger than the wavelength values ($320\,\mathrm{nm}<\lambda<400\,\mathrm{nm}$), the geometric optics condition is widely fulfilled. Furthermore, since isotropic scattering can be assumed (Brandi, 1998), the phase function can be made equal to one ($p(\mu_0)=1$), so indicating that the contribution of the in-scattering does not depend on direction or, in other words, that any radiation beam has the same probability to be scattered in the μ direction no matter from which direction μ' it is coming from (Ozisik, 1973).

3.1. A first-solution approach

A very simple solution method for the RTE for a one-dimensional, plane parallel system, assuming isotropic scattering was proposed by Shuster (Modest, 1993) and Schwarzschild (Kortüm, 1969). In this approach the total incident radiation G_λ at a given position x is divided into two, forward and backward hemispheres (G_λ^+ and G_λ^-),

according to the following integrals:

$$G_\lambda^+ = 2\pi \int_{\mu=0}^{\mu=1} I_\lambda^+(x,\mu')\,\mathrm{d}\mu' \quad \text{for } 0<\mu\leqslant 1, \tag{5a}$$

$$G_\lambda^- = 2\pi \int_{\mu=1}^{\mu=0} I_\lambda^-(x,\mu')\,\mathrm{d}\mu' \quad \text{for } -1\leqslant\mu<0, \tag{5b}$$

where $I_\lambda^+(x,\mu)$ and $I_\lambda^-(x,\mu)$ stand for the radiation intensities at any given position x in the μ direction, for each of the corresponding forward ($0<\mu\leqslant 1$) and backward ($-1\leqslant\mu<0$) hemispheres, respectively.

By utilizing these definitions, Eq. (2) can be cast into a pair of coupled expressions, after averaging the intensities $I_\lambda^+(x,\mu)$ and $I_\lambda^-(x,\mu)$ over all possible μ directions on each hemisphere, hereby obtaining the following ordinary coupled equations for the G_λ^+ and G_λ^- functions, where the quotient $\omega_\lambda=\sigma_\lambda/\beta_\lambda$ (known as the spectral albedo) is used (Modest, 1993; Kortüm, 1969):

$$\frac{1}{2}\frac{\mathrm{d}G_\lambda^+}{\beta_\lambda\,\mathrm{d}x} + G_\lambda^+ = \frac{\omega_\lambda}{2}(G_\lambda^+ + G_\lambda^-), \tag{6a}$$

$$\frac{1}{2}\frac{\mathrm{d}G_\lambda^-}{\beta_\lambda\,\mathrm{d}x} + G_\lambda^- = \frac{\omega_\lambda}{2}(G_\lambda^+ + G_\lambda^-). \tag{6b}$$

Several solutions have been proposed for these equations. The most generally accepted in the field of diffuse reflectance is the hyperbolic solution of Kubelka–Munk (K–M) (Kortüm, 1969), which is adopted in this work for data processing. Two relevant relationships emerge from this solution:

$$\frac{(R_{\infty,\lambda}-1)^2}{2R_{\infty,\lambda}} = \frac{K_\lambda}{S_\lambda} \tag{7}$$

and

$$S_\lambda\, d = \frac{1}{b}\left(\sinh^{-1}\frac{b}{T_\lambda}\right) + \ln\, R_{\infty,\lambda}$$
$$\text{being } b = \frac{1}{2}\left(R_{\infty,\lambda} - \frac{1}{R_{\infty,\lambda}}\right), \tag{8}$$

where $S_\lambda = 2\sigma_\lambda$, $K_\lambda = 2\kappa_\lambda$, $T_\lambda = G^+_{\lambda(x=0)}/G^+_{\lambda(x=d)}$ (T_λ=medium 'transmittance') and $R_{\infty,\lambda}=G^+_{\lambda(x=0)}/G^-_{\lambda(x=0)}$ ($R_{\infty,\lambda}$ = reflectance of the layer at $x=0$ when the medium is so optically thick that the reflectance is indifferent to d, condition that was always fulfilled when the fluidized bed was made with the catalyst composite, at all tested expansions).

A critical assumption in the original derivation of the approximate solution of K–M is the requirement of diffuse irradiation on the sample (Kortüm, 1969). However, its conclusions can be extended to cases of collimated irradiation, provided that multiple, isotropic angular distribution of scattering is quickly established inside the participating medium, as happens in our case.

3.2. Estimation of the optical parameters by using the DOM in an unidirectional and unidimensional model (1DD)

As said before, radiation transport through a participative medium (which may imply absorption, scattering and chemical reaction) is, in general, highly complex. Consequently, its mathematical description has analytical solution only for very simplified situations. Nevertheless, among the many numerical approximations that have been tried it is generally recognized that the DOM, developed in the frame of the generalized transport theory (Duderstadt and Martin, 1979) is one of the most powerful tools for the solution of a wide variety of +'practical' radiation transport problems. It allows solving the RTE by transforming the integro-differential equation system into an algebraic combination of discrete ordinate equations, by taking account of the functional and directional dependency of the propagation phenomena.

Each integro-differential equation is valid for a certain propagation direction ($\underline{\Omega}$). Hence, the DOM reduces all possible directions to a bunch of them, as a representative sample of the whole solid angle. In other words, the solid angle defined as the area of a sphere of unit radius (4π) is divided into a number of elements of solid angles. Each element is characterized by one central direction and by one element of area of the unit sphere (weight factor). For each of these chosen directions ($\underline{\Omega}_j$) a discrete ordinate equation is obtained. The weight factors and the director cosines can be calculated according to Duderstadt et al. criteria (Duderstadt and Martin, 1979). The integro-differential RTEs, so transformed into an algebraic system of discrete ordinate equations (one for each considered direction), are then coupled by the in-scattering function (the source function) and solved by the Gauss quadrature method.

In addition, the solution of the RTE by any numerical method requires not only to establish or define the boundary conditions but also to know the phase function and the optical parameters (viz., the spectral scattering and absorption coefficients). Conversely, these parameters can be the output of the calculations, as in the present case.

Summarizing, according to the DOM guidelines, the problem can be thought as a bunch of collimated uniform radiation beams absorbed and scattered by the fluidized bed inside the cell, after crossing the front cell wall. In a simplified unidimensional model it can be assumed that only a (virtual) cylindric volume is illuminated by the uniform beams within the cell, while the rest of the bed space is

radiationless. This assumption allows one to consider any beam to evaluate both the spectral transmittance (T_λ) and reflectance (R_λ), defined in this case, respectively, as

$$T_\lambda = \frac{q^+_{n,\lambda}(x=d)}{q^+_{n,\lambda}(x=0)} \quad \text{and} \quad R_\lambda = \frac{q^-_{n,\lambda}(x=0)}{q^+_{n,\lambda}(x=0)}, \tag{9}$$

being:

$$q^+_{n,\lambda}(x) = \int_{\Omega^+} I_\lambda(x, \underline{\Omega})\underline{\Omega}\cdot\underline{n}\,\mathrm{d}\Omega, \tag{10}$$

$$q^-_{n,\lambda}(x) = \int_{\Omega^-} I_\lambda(x, \underline{\Omega})\underline{\Omega}\cdot\underline{n}\,\mathrm{d}\Omega, \tag{11}$$

the radiation fluxes in the direction $\underline{n}$, perpendicular to the cell wall surfaces.

Since for each wavelength, both the diffuse reflectance and transmittance of the fluidized bed (R_λ and T_λ) are experimental, and independently measured, the spectral optical coefficients β_λ (extinction) and κ_λ (absorption) can be determined by incorporating the DOM equation set as a subroutine to a computational program for nonlinear parameters estimation. The program searches for the pair of parameters that minimize the quadratic differences between the experimental diffuse transmittance and reflectance values, and those defined and calculated by the model.

Hence, the optical parameter σ_λ and κ_λ of the FB were estimated by applying the DOM to solve Eq. (2), based on a 1DD model. Compared vis-a-vis with the K–M approximation, which considers only two plane-uniform incident (forward) and reflected (backward) hemispherical incident radiations, the DOM performs the integration by weighting the radiation intensities for each direction. This advantage is particularly useful when a finite, 'disc-size' collimated beam is the experimental boundary condition for the incident radiation, as in our set-up.

3.3. Verification of the estimated parameters by a bi-directional and two-dimensional (2DD) solution method for the RTE

The appropriateness of the estimates of the spectral optical parameters of the narrow-channel FB calculated by the above-described DOM (1DD) method was verified by using them in a more complex 2D model. This kind of modeling admits that lateral dispersion of the beams may be significant. In such a case, the irradiated volume would not be limited to just a directly illuminated cylinder, but it would also spread out to a more extended 'diffusely irradiated' domain, well outside said portion of the cell.

Essentially, in the 2D (x, y) modeling the cell was considered as a thin rectangular parallelepiped containing the fluidized bed and limited by two radiation transparent parallel planes. As in the model for one dimension (x), a circular collimated radiation beam impinges upon one of the limiting planes and the propagation of radiation inside the bed maintained the two directional spherical coordinates (θ, ϕ). The RTE for a 2D, rectangular and participative medium can then be written as

$$\mu\frac{\partial I_\lambda(x, y, \underline{\Omega})}{\partial x} + \eta\frac{\partial I_\lambda(x, y, \underline{\Omega})}{\partial y} = -(\kappa_\lambda + \sigma_\lambda) I_\lambda(x, y, \underline{\Omega}) + \frac{\sigma_\lambda}{4\pi}\int_{4\pi} p(\underline{\Omega}' \to \underline{\Omega}) I_\lambda(x, y, \underline{\Omega}')\,\mathrm{d}\Omega', \tag{12}$$

where μ and η are the director cosines of the $\underline{\Omega}$ direction with respect to the x and y cartesian axes ($\mu = \cos\phi\sin\theta$, $\eta = \sin\phi\sin\theta$), while the RTE boundary conditions are given by

Irradiated wall:

Illuminated area:

$$I_\lambda(y_1 \leqslant y \leqslant y_2, x = 0, \underline{\Omega} = \underline{\Omega}_{\text{in,haz}}) = I^0_\lambda, \tag{13a}$$

$$I_\lambda(0 \leqslant y < y_1, x = 0, \underline{\Omega} = \underline{\Omega}_{\text{in}}) = 0, \tag{13b}$$

Non-illuminated area:

$$I_\lambda(D_B/2 \geqslant y > y_2, x = 0, \underline{\Omega} = \underline{\Omega}_{\text{in}}) = 0, \tag{13c}$$

Rest of the walls:

Non-illuminated area:

$$I_\lambda(y = 0, x, \underline{\Omega} = \underline{\Omega}_{\text{in}}) = 0, \tag{13d}$$

$$I_\lambda(y = D_B/2, x, \underline{\Omega} = \underline{\Omega}_{\text{in}}) = 0, \tag{13e}$$

$$I_\lambda(y, x = d, \underline{\Omega} = \underline{\Omega}_{\text{in}}) = 0. \tag{13f}$$

In this case, all of the integro-differential equations (one for each considered direction) were discretized by applying central finite-differences to a space divided into cells. The "in scattering" source term was calculated by a numerical integration. Each one of the so obtained algebraical equations, was coupled by the quadrature term or source term which in order to be calculated needs, in turn, the intensities of radiation for all the rest of directions. Hence, an iteration was applied to find the solution for the radiation balance in a given direction—and for each of the spatial cells-, by taking into account all the angular contributions. As said before, the spectral optical coefficients (σ_λ and κ_λ) previously estimated with the unidirectional uni-dimensional model, were introduced here as fixed model parameters.

Once the radiation intensities for each given direction, $I_\lambda(x, y, \underline{\Omega})$, were known, they were integrated to obtain the net radiative fluxes, or irradiances, either positive (forward, from the irradiated wall to the opposite), or negative (backward, from the opposite to the front irradiated wall):

$$q^+_{n,\lambda}(x, y) = \int_{\Omega^+} I_\lambda(x, y, \underline{\Omega})\underline{\Omega}\cdot\underline{n}\,\mathrm{d}\Omega, \tag{14a}$$

$$q^-_{n,\lambda}(x, y) = \int_{\Omega^+} I_\lambda(x, y, \underline{\Omega})\underline{\Omega}\cdot\underline{n}\,\mathrm{d}\Omega. \tag{14b}$$

From the calculation of these net fluxes the transmittance (T_λ) and reflectance (R_λ) of the fluidized bed,

Table 1
Comparison between the estimates of transmittance and reflectance of a seven-fold expanded (Ex 7) fluidized bed of titania CVD–coated quartz sand photocatalyst, obtained with a 2DD DOM, and experimental values[a]

Wavelength (nm)	Percent transmittance $T_\lambda\% = \frac{\langle q^+_{n,\lambda}(x=d,y)\rangle_{A_{out}}}{\langle q^+_{n,\lambda}(x=0,y)\rangle_{A_{in}}} \times 100$		Percent reflectance $R_\lambda\% = \frac{\langle q^-_{n,\lambda}(x=0,y)\rangle_{A_{in}}}{\langle q^+_{n,\lambda}(x=0,y)\rangle_{A_{in}}} \times 100$		Percent extinctance $E_\lambda\% = (1-T_\lambda)\times 100$	
	Experimental	2DD model	Experimental	2DD model	Experimental	2DD model
320	1.60	1.08	3.66	3.67	98.4	98.9
350	3.69	3.04	6.77	6.91	96.3	97.0
380	13.1	11.7	16.0	15.4	86.9	88.3

[a]Using the spectral optical parameters previously obtained with the DOM (1DD) method.

defined as

$$T_\lambda = \frac{\langle q^+_{n,\lambda}(x=d,y)\rangle_{A_{out}}}{\langle q^+_{n,\lambda}(x=0,y)\rangle_{A_{in}}}$$

$$\text{and} \quad R_\lambda = \frac{\langle q^-_{n,\lambda}(x=0,y)\rangle_{A_{in}}}{\langle q^+_{n,\lambda}(x=0,y)\rangle_{A_{in}}}, \tag{15}$$

were evaluated, being:

$$\langle q^+_{n,\lambda}(x=d,y)\rangle_{A_{out}} = \frac{1}{A_{out}}\int_{A_{out}} q^+_{n,\lambda}(x=d,y)\,dA = \frac{1}{D_B/2}\int_0^{D_B/2} q^+_{n,\lambda}(x=d,y)\,dy, \tag{16a}$$

$$\langle q^-_{n,\lambda}(x=0,y)\rangle_{A_{in}} = \frac{1}{A_{in}}\int_{A_{in}} q^-_{n,\lambda}(x=0,y)\,dA = \frac{1}{D_B/2}\int_0^{D_B/2} q^-_{n,\lambda}(x=0,y)\,dy, \tag{16b}$$

$$\langle q^+_{n,\lambda}(x=0,y)\rangle_{A_{in}} = \frac{1}{A_{in}}\int_{A_{in}} q^+_{n,\lambda}(x=0,y)\,dA = \frac{1}{D_B/2}\int_0^{D_B/2} q^+_{n,\lambda}(x=0,y)\,dy. \tag{16c}$$

These calculated T_λ and R_λ values are compared with the experimental data in Table 1. (More details about the treatment of 2D models and solution methods are given in Brandi et al. (1996, 1999) and Romero et al. (1997).

4. Results and discussion

In Figs. 3 and 4 the experimental measurements of the percent spectral reflectance ($R_\lambda\%$) and transmittance ($T_\lambda\%$) registered in spheres R and T, respectively, as a function of wavelength are presented for both the bare quartz sand and the photocatalyst composite at the three different expansions of the fluidized bed that were tested (Ex 7, Ex 6 and Ex 5).

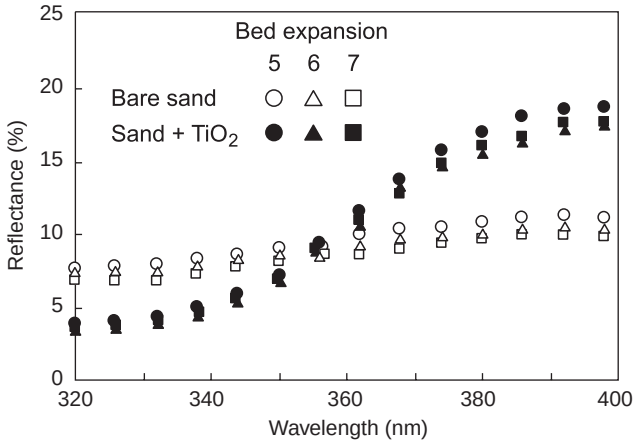

Fig. 3. Experimental values of the percent spectral reflectance ($R_\lambda\%$) as a function of wavelength, of bare and titania CVD–coated quartz sand, for three different expansions of the fluidized bed tested.

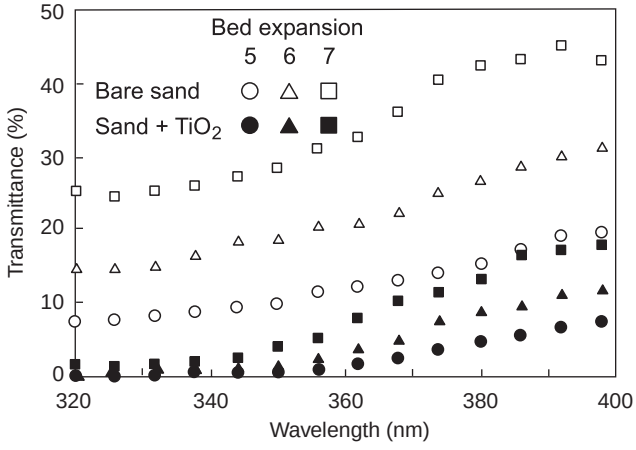

Fig. 4. Experimental values of the percent spectral transmision ($T_\lambda\%$) as a function of wavelength, of bare and titania CVD–coated quartz sand, for three different expansions of the fluidized bed tested.

As it can be appreciated in Fig. 3, the $R_\lambda\%$ slightly decreased with bed expansion for both materials but it was dependent on wavelength for the titania-coated quartz sand FB, following the typical wavelength absorption profile of

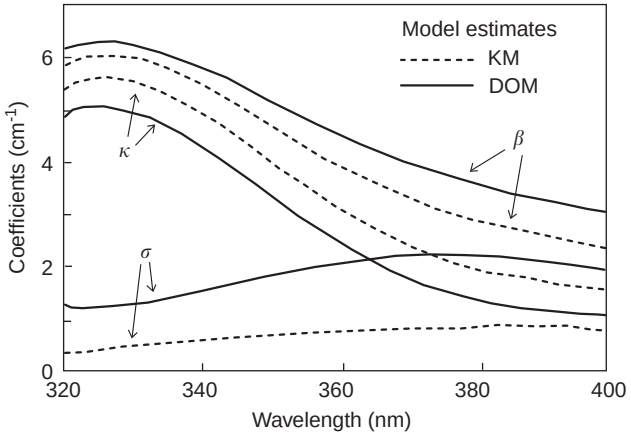

Fig. 5. Calculated values of the spectral scattering (σ_λ), absorption (κ_λ) and extinction (β_λ) coefficients ($\beta_\lambda = \sigma_\lambda + \kappa_\lambda$), obtained using the K–M and the discrete ordinate one-dimensional DOM (1DD) models for an Ex 7 fluidized bed of the photocatalytic composite (titania CVD–coated quartz sand).

TiO_2. The FB of bare quartz sand behaved, on the other hand, as an almost-gray reflectant media. While the bed expansion appears to be inconsequential to R_λ% for the two materials, the T_λ% increased in both cases as a function of wavelength (Fig. 4) *and* fluidized bed expansion, indicating that not only the TiO_2 was an UV radiation absorbent but, also, that the bare quartz sand (a natural product) was active, albeit at lower scale than the titania-coated sand, a behavior already reported in previous works (Pozzo et al., 1999, 2000).

The calculated values of the spectral scattering (σ_λ) and absorption (κ_λ) coefficients, and their additive optical parameter, the extinction coefficient β_λ, obtained by using both the coarser K–M approach and the more refined DOM (1DD model) for the fluidized bed of the photocatalytic composite at Ex 7, are depicted in Fig. 5. (The estimated values for Ex 6 and Ex 5 beds followed similar patterns.) It is significant to note, firstly, that the pairs of calculated values for each coefficient, estimated by both methods, are within the same order of magnitude and follow a similar profile as a function of wavelength. However, the extinction coefficients (β_λ) obtained by the two methods differ. This can be explained (recalling that radiation 'extinction' compounds absorptive-dispersive optical phenomena) by recognizing that part of the incoming radiation is necessarily lost by out-scattering, outside the hypothetical optical cylinder within which the radiation travels between both spheres. Said "lost" energy, which is not registered by sphere T, is accounted for in different manners by both methods.

Certainly, since uniform conditions for any point located on each parallel plane perpendicular to the cell walls are assumed in both the K–M and the DOM (1DD) methods, this lost radiation is "formally ignored" by them. However, the K–M solution minimizes the impact of scattering and at the same time "overestimates" the impact of radiation absorption upon extinction, as indicated by the individual coefficients shown in Fig. 5. This is a direct consequence of the combination of (a) the isotropic scattering assumption and (b) the averaging for the direction-dependent radiation intensities into only one horizontal direction, that the K–M method makes. In other words since by hypothesis all the out-scattered radiation has the same probability of being returned by in-scattering, the resulting extinction is assigned by the K–M method to a more absorbent (but less dispersive) media.

In the calculation *via* DOM (1DD model), on the other hand, isotropic scattering is also assumed but the beam direction is considered as a variable to integrate the intensities. Hence, the in-scattering contribution of the zones located out of the "virtual illuminated cylinder" is ignored and, so, in-scattering is underestimated (i.e., in the DOM model the fluidized is predicted to be less absorptive and more dispersive).

An improvement in the estimation of the optical parameters of the FB can be surely obtained with the more realistic DOM two-directional (2DD) model. Since this is a highly consuming method of computing resources, it was employed here only to validate the estimates of the optical parameters calculated by the 1DD model. In Table 1 the calculated values of T_λ% and R_λ% (calculated by using the 2DD model with the σ_λ and κ_λ spectral parameters obtained with the 1DD model) together with the predicted extinctance, $E_\lambda\% = (1 - T_\lambda) \times 100$ are compared with the experimentally measured data, for three relevant wavelengths: 320, 350 and 380 nm.

A close agreement between calculated and experimental values is observed in Table 1, particularly in regards to R_λ%. Again, the 'somewhat lower than experimental' values obtained for T_λ% by using the optical parameters calculated by the 1DD model, would be a consequence that in this model the out-scattered radiation (out of the borders of the directly illuminated zone) was ignored in the 1DD evaluation of the coefficient. However, this 'lateral dispersion' was found to be relatively negligible, for the highest λ (near-visible zone) of the computational runs. This can be appreciated in Fig. 6 where the radiation field profiles inside the cell containing an Ex 7 fluidized bed of the titania-coated sand are presented as the ratios between either the net forward (positive) or backward (negative) radiation fluxes and the entering radiation flux, for the above cited wavelengths (320, 350 and 380 nm), by using the 1DD optical parameters as input for the 2DD model calculations.

All things considered these results suggest that a DOM(1DD) model is accurate enough for the modeling of FB of the titania–quartz sand composite in order to evaluate their optical parameters, with the obvious saving in computational resources that this choice implies. Still, a 2D model is a good option for the modeling of the radiation field inside a photochemical reactor once said optical parameters are known. The coarser K–M model yields fair order-of-magnitude estimates for the spectral

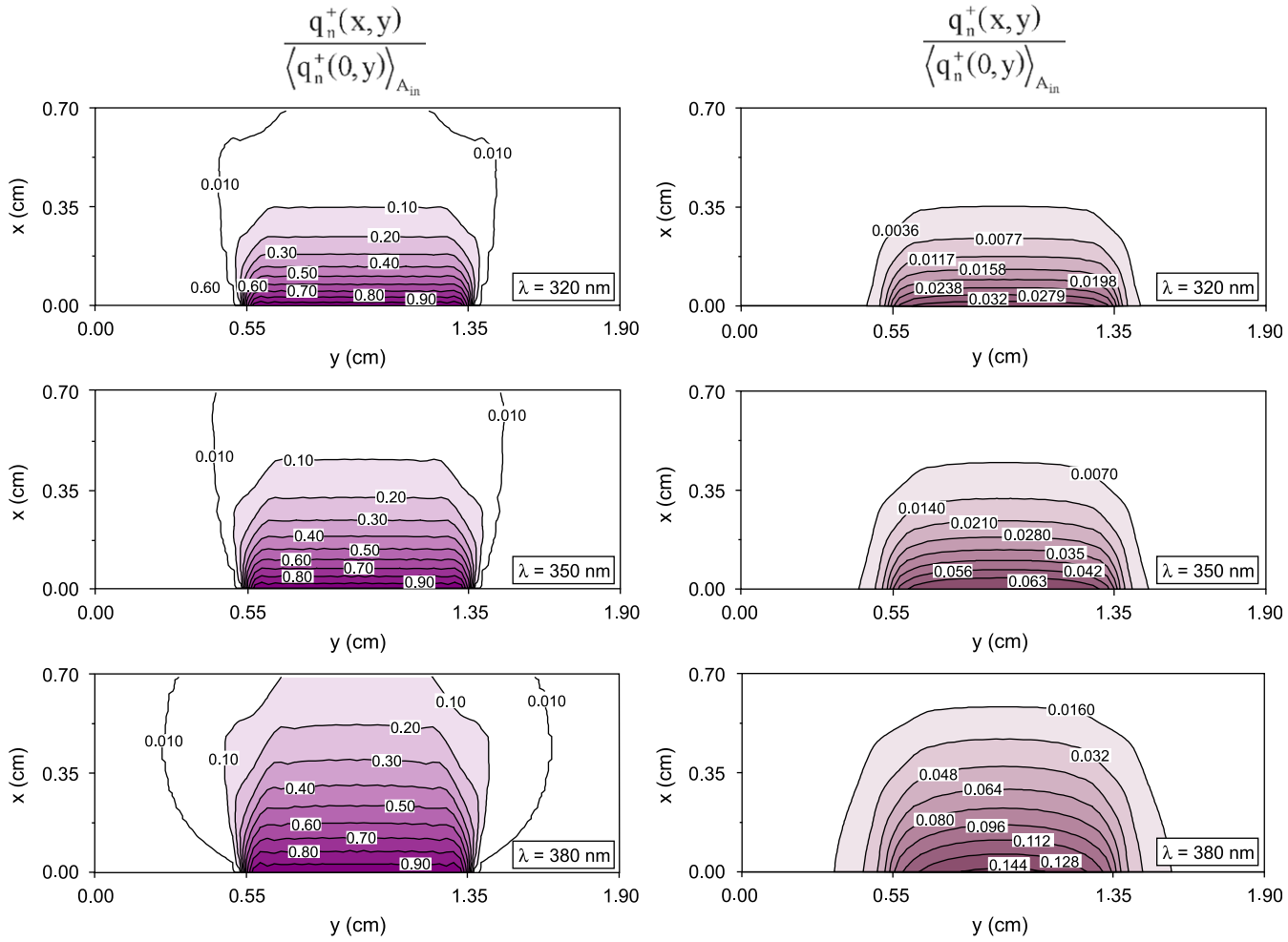

Fig. 6. Radiation field profiles inside the cell containing an Ex 7 fluidized bed of the titania CVD–coated quartz sand, presented as the ratios between the net forward (positive) or backward (negative) radiation fluxes and the entering radiation flux, for selected wavelengths, obtained by using the DOM (1DD) optical parameters as input of the 2DD model.

extinctance, but strongly minimizes the impact of scattering, though.

Finally, by taking into account that for any given loading of photocatalyst the bed expansion is inversely related to photocatalyst concentration in the two-phase media, we tested whether *specific* (i.e., per mass or volume fraction of the solid phase) optical parameters of the FB could be (or had been) obtained. So, the resulting products of the absorption, scattering and extinction coefficients calculated by both the KM and DOM methods multiplied by the corresponding bed expansions (that is, spectral coefficient × Ex #) as a function of wavelength, are presented in Fig. 7. The three expansion-averaged values for both methods are also represented in the diagram as doted and continuous lines, respectively. It can clearly be appreciated that the individual values of the products for each set are very close among them and to the averaged values. This encouraging finding is an indication that the combined products (coefficient × Ex #) are *specific* volumetric values with direct application for engineering design.

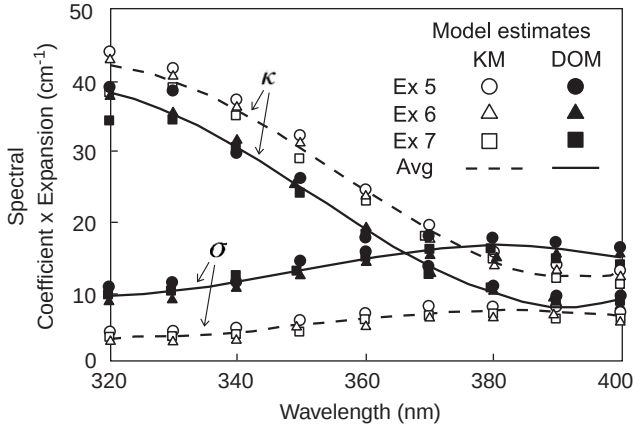

Fig. 7. Products of the absorption, scattering and extinction coefficients calculated by both the KM and DOM methods multiplied by the corresponding bed expansions (spectral coefficient × Ex #) as a function of wavelength, for the FB of titania CVD–coated quartz sand. The expansion-averaged values for both methods are also shown, as dashed and continuous lines, respectively.

5. Conclusions

It has been shown that the relevant spectral optical parameters (spectral absorption and scattering coefficients) of narrow-channel fluidized beds of a granular photocatalytic composite, made of titania deposited onto quartz sand by plasma-CVD, can be quantified using a planar cell together with a pair of integrating spheres and a colimated, monochromatic light beam. The parameters obtained by using the discrete ordinate method in an unidimensional and unidirectional model are accurate enough for the modeling of the radiation field inside this type of photocatalytic reactors, instead of the more involved and computationally demanding two and/or 3-D methods.

Acknowledgements

The authors thank the financial support from the Consejo Nacional de Invetigaciones Científicas y Técnicas (CONICET), Universidad Nacional del Litoral (UNL) and Agencia Nacional de Promoción Científica y Tecnológica (ANPCyT) of Argentina. Thanks are also given to Eng. Claudia Romani for her technical assistance.

References

Brandi, R.J., 1998. Modeling of the radiation field in a flat heterogeneous reactor for the photacatalytical decomposition of water contaminants. Ph.D. Dissertation, Universidad Nacional del Litoral, Santa Fe, Argentina, pp. 207–230.

Brandi, R.J., Alfano, O.M., Cassano, A.E., 1996. Modeling of radiation absorption in a flat plaste photocatalytic reactor. Chemical Engineering Science 51 (11), 3169–3174.

Brandi, R.J., Alfano, O.M., Cassano, A.E., 1999. Rigorous model and experimental verification of the radiation field in a flat solar collector simulator employed for photocatalytic reactions. Chemical Engineering Science 54, 2817–2827.

Duderstadt, J.J., Martin, R., 1979. Transport Theory. Wiley, New York.

Karches, M., Morstein, M., Pozzo, R.L., Giombi, J.L., Baltanás, M.A., 2002. Plasma-CVD-coated glass beads as photocatalyst for water decontamination. Catalysis Today 72, 267–279.

Kortüm, G., 1969. Reflectance Spectroscopy. Springer, New York.

Modest, M.F., 1993. Radiative Heat Transfer. McGraw-Hill, New York.

Ozisik, M.N., 1973. Radiative Transfer and Interactions with Conduction and Convection. Wiley, New York.

Pozzo, R.L., Baltanás, M.A., Cassano, A.E., 1999. Towards a precise assesment of the performance of supported photocataslysts for water detoxification process. Catalysis Today 54 (1), 143–157.

Pozzo, R.L., Giombi, J.L., Baltanás, M.A., Cassano, A.E., 2000. The performance in a fluidized bed reactor of photocatalysts immobilized onto inert supports. Catalysis Today 62, 175–187.

Romero, R.L., Alfano, O.M., Cassano, A.E., 1997. Cylindrical photocatalytic reactors. Radiation absortion and scattering effects produced by suspended fine particles in an annular space. Industrial and Engineering Chemistry Research 36, 3094–3109.